A systematic investigation of the performance of copper-, cobalt-, iron-, manganese-, and nickel-based oxygen carriers for chemical looping combustion technology through simulation studies

MUKHERJEE, Sanjay, KUMAR, Prashant, YANG, Aidong and FENNELL, Paul

Published version

MUKHERJEE, Sanjay, KUMAR, Prashant, YANG, Aidong and FENNELL, Paul (2015). A systematic investigation of the performance of copper-, cobalt-, iron-, manganese-, and nickel-based oxygen carriers for chemical looping combustion technology through simulation studies. Chemical Engineering Science, 130, 79-91.

Chemical Engineering Science 130 (2015) 79–91

Contents lists available at ScienceDirect

Chemical Engineering Science

journal homepage: www.elsevier.com/locate/ces

A systematic investigation of the performance of copper-, cobalt-, iron-, manganese- and nickel-based oxygen carriers for chemical looping combustion technology through simulation models

Sanjay Mukherjee [a], Prashant Kumar [a,*], Aidong Yang [b], Paul Fennell [c]

[a] Department of Civil and Environmental Engineering, University of Surrey, Guildford, Surrey GU2 7XH, United Kingdom
[b] Department of Engineering Science, University of Oxford, Parks Road, Oxford OX1 3PJ, United Kingdom
[c] Department of Chemical Engineering, Imperial College London, South Kensington, London SW7 2AZ, United Kingdom

HIGHLIGHTS

- The performance of five different types of oxygen carriers for CLC is analysed.
- Energy penalty and net electrical efficiency for CO_2 capture is calculated.
- CLC process was compared with other capture technologies.
- Iron oxides achieve highest electrical efficiency of 34.3% with ~100% CO_2 capture.
- Demonstrated relation between reaction enthalpy of oxygen carrier and power output.

GRAPHICAL ABSTRACT

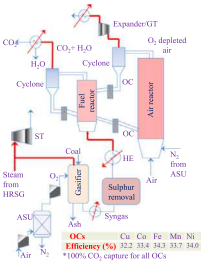

ARTICLE INFO

Article history:
Received 3 September 2014
Received in revised form
15 February 2015
Accepted 2 March 2015
Available online 17 March 2015

Keywords:
IGCC-CLC process
CO_2 capture
Oxygen carriers
Reaction enthalpy

ABSTRACT

The Integrated Gasification Combined Cycle coupled with chemical looping combustion (IGCC-CLC) is one of the most promising technologies that allow generation of cleaner energy from coal by capturing carbon dioxide (CO_2). It is essential to compare and evaluate the performances of various oxygen carriers (OC), used in the CLC system; these are crucial for the success of IGCC-CLC technology. Research on OCs has hitherto been restricted to small laboratory and pilot scale experiments. It is therefore necessary to examine the performance of OCs in large-scale systems with more extensive analysis. This study compares the performance of five different OCs – copper, cobalt, iron, manganese and nickel oxides – for large-scale (350–400 MW) IGCC-CLC processes through simulation studies. Further, the effect of three different process configurations: (i) water-cooling, (ii) air-cooling and (iii) air-cooling along with air separation unit (ASU) integration of the CLC air reactor, on the power output of IGCC-CLC processes – are also investigated. The simulation results suggest that iron-based OCs, with 34.3% net electrical efficiency and ~100% CO_2 capture rate lead to the most efficient process among all the five studied OCs. A net electrical efficiency penalty of 7.1–8.1% points leads to the IGCC-CLC process being more efficient than amine based post-combustion capture technology and equally efficient to the solvent based pre-combustion capture technology. The net electrical efficiency of the IGCC-CLC process increased by 0.6–2.1% with the use of air-cooling and ASU integration, compared with the water- and air-cooling cases. This work successfully demonstrates a correlation between the reaction enthalpies of different OCs and power output, which suggests that the OCs with higher values of reaction enthalpy for oxidation ($\Delta H_{r,\ oxidation}$) with air-cooling are more valuable for the IGCC-CLC.

* Corresponding author. Tel.: +44 1483 682762; fax: +44 1483 682135.
E-mail addresses: P.Kumar@surrey.ac.uk, Prashant.Kumar@cantab.net (P. Kumar).

http://dx.doi.org/10.1016/j.ces.2015.03.009

1. Introduction

The Intergovernmental Panel on Climate Change (IPCC) has outlined the threat from unabated anthropogenic carbon dioxide (CO_2) emissions through their adverse effects on the global climate. This leads to a requirement to minimise CO_2 emissions, particularly from fossil fuel (e.g. pulverised coal, PC) power plants (IPCC, 2013, 2014). These power plants also emit sulphur dioxide (SO_2) and particulate matter that cause air and water pollution, and thus affect public health (Kumar and Saroj, 2014). In the past few decades, scientific research communities and policy makers around the globe have shown interest in replacing traditional fossil fuel conversion technologies in order to mitigate climate change and environmental pollution (IEA, 2013; Leung et al., 2014; Pires et al., 2011). An integrated gasification combined cycle coupled with a chemical looping combustion (IGCC-CLC) process is considered to be one of the most promising fuel, in particular coal, conversion methods for electricity production and CO_2 capture (Cormos, 2012; Erlach et al., 2011; Li and Fan, 2008; Mukherjee et al., 2014). In the IGCC-CLC process, coal is gasified to produce syngas, which mainly contains carbon monoxide (CO) and hydrogen (H_2). Syngas is then supplied to the fuel reactor of the CLC system where it is oxidised to CO_2 and steam (H_2O) by an oxygen carrier (OC), as shown in Fig. 1 (Lyngfelt et al., 2001). The OC is made of metals with different oxidation states and carries oxygen to the fuel reactor for syngas combustion (Lyngfelt et al., 2001). The OC is re-oxidised/regenerated in the air reactor, before being recycled to the fuel reactor. In this way, a series of oxidation–reduction cycles are repeated, with the OC circulated within the CLC system for a certain number of cycles depending on its chemical and physical characteristics, such as reactivity, mechanical strength and thermal stability. The flue gas stream from the CLC system comprises almost entirely CO_2 and H_2O; H_2O can easily be separated by simple condensation, and CO_2 is sent for storage and compression (Chiesa et al., 2005).

The OCs are the foundation of CLC and are considered as a decisive factor to incorporate CLC in commercial operations for carbon capture and storage (CCS) (Bhavsar et al., 2014; Boot-Handford et al., 2014; Fang et al., 2009; Hossain and de Lasa, 2008; Lyngfelt et al., 2008). A significant quantity of *laboratory* and *pilot scale* studies have been conducted in the past years on development, testing performance enhancement and selection of OCs for CLC (Adanez et al., 2004, 2012; de Diego et al., 2014; Gao et al., 2008; Imtiaz et al., 2013). For instance, Jing et al. (2013) investigated the reactivity of three groups of OCs developed by using different combinations of metals such as copper, iron, manganese, magnesium and titanium. The new materials developed in their study showed promising results as OCs, with sufficient mechanical strength and high reactivity with methane (CH_4). Cabello et al. (2014) studied the kinetic parameters of an alumina impregnated iron-based OC for gaseous fuels. A total solid inventory of 150 kg/MW was utilised in their study, which showed high reactivity for the iron-based OC. Performance of different manganese ores for CLC was evaluated by Arjmand et al. (2014) suggesting manganese could be an interesting material for solid fuels due to its high char conversion rates. Imtiaz et al. (2013) reviewed the synthesis strategies followed to develop new OC materials and studied the physical and chemical properties of the newly developed OCs. A large set of data is available comparing different OCs based on the outcomes of *laboratory and pilot* scale experiments that focused primarily on reaction kinetics, cost and conversion efficiency (Adánez et al., 2004; Cho et al., 2004; de Diego et al., 2014; Fossdal et al., 2011; Imtiaz et al., 2013; Wolf et al., 2005).

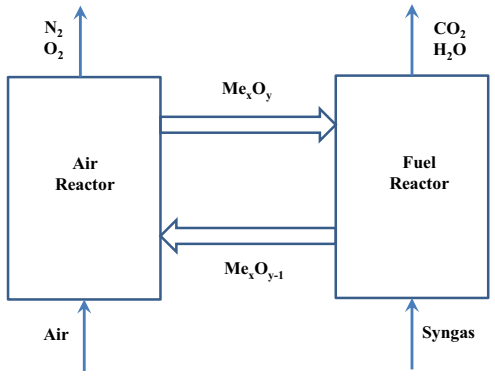

Fig. 1. Flow of materials through air and fuel reactors of a typical CLC reactor system (Lyngfelt et al., 2001).

It is equally important to analyse the performance of OCs for *large or industrial scale* CLC systems, but only a handful of such investigations are available (Table 1). For instance, Anheden and Svedberg (1996) and Anheden (2000) compared the performance of iron-, nickel- and manganese-based OCs for IGCC with CLC process and found very similar power outputs (for all three OCs) with reference to an IGCC with conventional combustion process. Anheden and Svedberg (1998) provided a detailed exergy analysis of the CLC process with nickel- and iron-based OCs, using methane and syngas separately as fuel, and compared the exergetic power efficiencies with a conventional conversion process. They found the CLC process to have higher exergetic power efficiencies compared with the conventional conversion process, with the iron-based OC being the most efficient. The above three studies performed comparison analysis based on an estimated power output, efficiency value and physical exergies. The actual power output was out of the scope of their work, which is considered for investigation in our study. In addition, these studies do not consider CO_2 compression and energy consumption in the gasification island – these aspects are analysed in detail in our work.

Rezvani et al. (2009) studied a double stage CLC system with nickel-based OC, and obtained an electrical efficiency of 35.2%. Cormos (2010b) examined the performance of CLC, using iron oxide as an OC, in conjunction with a co-gasification process of coal and biomass with CCS. The work showed that CLC with a co-gasification process could achieve an overall electrical efficiency of 38.82%. Another study by Cormos (2012) suggests that CLC using iron-based OC is more energy efficient for CO_2 capture than physical absorption processes. Erlach et al. (2011) carried out a sensitivity analysis on CLC, which used nickel-based OC with different expander (also referred as gas turbine or GT in our study) inlet temperatures. Their results indicated that the OCs with higher thermal stability could provide potential efficiency advantages for CLC.

Most of the existing studies on *large scale* CLC system modelling have examined iron and nickel oxides as OCs (Cormos, 2012; Erlach et al., 2011; Rezvani et al., 2009; Sorgenfrei and Tsatsaronis, 2014). The research on other common OCs such as manganese, cobalt and copper oxides is mainly confined to *laboratory* or *pilot* scale experiments (Adánez et al., 2004; Arjmand, 2014; Cho et al., 2004; de Diego et al., 2004; Hossain and de Lasa, 2007; Johansson et al., 2006b). Shulman et al. (2009) investigated the performance of OCs prepared by mixing manganese oxides with iron, nickel and silicon oxides for chemical-looping with oxygen uncoupling (CLOU) in laboratory scale reactors. They found high reactivity for mixtures of manganese/iron oxides and manganese/nickel oxides with methane. Song et al. (2014) performed laboratory experiments to analyse the reactivity, stability and suitability of manganese, copper and cobalt oxides (at temperatures between 800 and 950 °C) for chemical looping air separation (CLAS) technology. Clearly, the existing literature lacks knowledge on the comparison of different OCs for *large-scale* CLC systems based on the same baseline assumptions for modelling. In this work, we focus on a systematic comparison of the performance of five most commonly

used metal-based OCs (i.e. copper, cobalt, iron, manganese and nickel oxides) for large-scale IGCC-CLC processes (Bao et al., 2014; Bhavsar et al., 2014; Jing et al., 2013; Shah et al., 2012; Song et al., 2014). The simulations assume a single basis of analysis with respect to selected fuel, production scale and modelling approach. This work also examines: (i) the effect of water-cooling, air-cooling and air separation unit (ASU) integration of the CLC air reactor on the power output, (ii) the role of reaction enthalpies in determining the performance of various OCs, and (iii) the net power penalty associated with the CO_2 capture in IGCC-CLC processes via comparison with a base case, which represents a conventional IGCC plant without CO_2 capture.

2. Methodology

Flowsheet models for IGCC-CLC processes were developed in Aspen Plus using five different types of OCs, based on copper, cobalt, iron, manganese and nickel oxides. Table 2 shows the oxidised and reduced form of these five OCs and their melting points. The agglomeration and sintering of the OC particles needs to be avoided since it reduces the reactivity of the OCs and directly affects the overall process output. Keeping this in mind, an operating temperature range of 750–950 °C was selected for the CLC reactors, which is suitable for all the five OCs and can maintain the OC reactivity for a longer duration by avoiding sintering, agglomeration and melting (Chiu and Ku, 2012; Jerndal et al., 2006; Shah et al., 2012; Song et al., 2014). Moreover, all the OCs are supported with 15% aluminium oxide (Al_2O_3) and 15% silicon carbide (SiC) by mass, which enhances their thermal, mechanical and physical properties and hence, keeps them stable for longer durations (Li et al., 2010). The performance of each type of OC is tested for three different configurations ("a–c"), as described below:

- Configuration "a": Water-cooling of the CLC air reactor.
- Configuration "b": Air-cooling of the CLC air reactor.
- Configuration "c": Air-cooling along with ASU integration of the CLC air reactor.

Firstly, five IGCC-CLC processes were developed using configuration "a" that considers water-cooling of the CLC air reactor; these processes are represented by Cases 1a–5a. The numbers "1–5" indicate the type of OC used (see Table 2) and "a" indicates configuration type "a". For example, the term 'Case 1a' is used to represent the case with a copper-based OC having configuration type "a". The above five IGCC-CLC processes (Cases 1a–5a) were then modified by replacing water-cooling of the air reactor (configuration "a") by air-cooling (configuration "b"), which are represented by Cases 1b–5b. Later, Cases 1b–5b were further modified by adding ASU integration of the CLC air reactor. These new cases come under configuration "c" and are represented by Cases 1c–5c. Fig. 2 shows the process flow diagram for the IGCC-CLC process with air-cooling and ASU integration. All three configurations are similar in design but use different OCs in the CLC reactors, which are represented by the numbers "1–5". Grouping of the five OCs along with the three configurations "a–c" gives 15 different cases. For all the IGCC-CLC processes modelled in this study, the selected output range was between 350 and 400 MW. The results on the performance of the five OCs along with the three configurations "a–c" for the IGCC-CLC process are discussed in Section 3.

The key information about the input parameters (such as flow rates, pressure, temperature, equipment efficiency and fuel composition) used in order to construct the Aspen Plus flowsheet models of the above-mentioned 15 cases, were collected from various literature sources and are shown in Tables 2–4. Table 3 provides the design assumptions considered to develop the flowsheet models in Aspen Plus for all the IGCC-CLC cases. Chemical and phase equilibrium based on Gibbs free energy minimisation is assumed to develop the gasifier and CLC reactor models in our simulations. Table 4 shows the physical and chemical properties of the Illinois#6 coal used as fuel in all the cases.

CLC reactors are designed with membrane walls (where applicable) to allow pressurised water flow for cooling (Sorgenfrei and Tsatsaronis, 2014). Section 2.1 describes the plant layout and operating conditions for all IGCC-CLC cases. Details of the steam

Table 1
Summary of studies on large-scale CLC processes for electricity production and CO_2 capture.

Study	Conversion technology used	Fuel type	OC used	Electrical efficiency (% LHV)	CO_2 capture efficiency (%)
Anheden (2000)	IGCC-CLC	Methane	Iron oxide	45.8	–
	IGCC-CLC	Methane	Nickel oxide	44.4	–
Rezvani et al. (2009)	IGCC-CLC	Coal	Nickel oxide	35.2	100
Cormos (2012)	IGCC-CLC	Coal	Iron oxide	31.9–38.3	99.5
Erlach et al. (2011)	IGCC-CLC	Coal	Nickel oxide	37.7–39.0[a]	~100
Fan et al. (2012)	CDCLC	Coal	Iron oxide	34.7[a]	~100
Spallina et al. (2013)	IGCC-CLC	Coal	Ilmenite	39.98	97.52
Spallina et al. (2014)	IGCC-CLC	Coal	Iron oxide	41.0	>97.0
Hamers et al. (2014)	IGCC-CLC	Coal	Nickel oxide	41.4	97.1
Sorgenfrei and Tsatsaronis (2014)	IGCC-CLC	Coal	Iron oxide	44.8	~90

Notes: CDCLC stands for coal direct chemical looping combustion.

[a] Efficiencies are calculated based on higher heating value (HHV) of the coal.

Table 2
Summary of OCs and operating conditions used in this study (Chiu and Ku, 2012; Cho, 2005; Shah et al., 2012).

Case number corresponding to a particular OC	OC used	Oxidised/reduced form	Fuel reactor temperature (°C)	Air reactor temperature (°C)	Melting point of metal (°C)
1	Copper	CuO/Cu	750	950	1085
2	Cobalt	CoO/Co	750	950	1495
3	Iron	Fe_2O_3/FeO	750	950	1538
4	Manganese	Mn_3O_4/MnO	750	950	1246
5	Nickel	NiO/Ni	750	950	1455

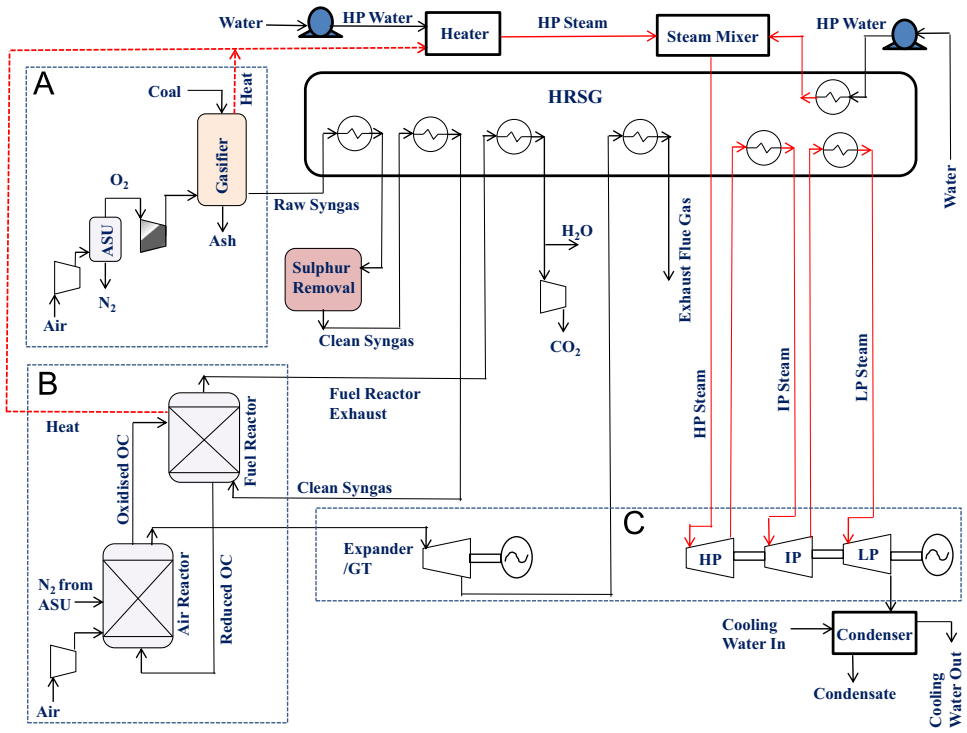

Fig. 2. Process flow diagram for IGCC-CLC process with air-cooling and ASU integration (configuration "c"). Sections "A", "B" and "C" represents "Gasification", "CLC" and "Power" Islands, respectively.

and water cycles for the IGCC-CLC processes are discussed in Section 2.2. Section 2.3 explains the development of complete process flowsheet models in Aspen Plus. Section S1 of the Supplementary Information (SI) explains the methodology and equations used to calculate the exergy of the process streams.

2.1. Plant layout and design for the IGCC-CLC process

This section describes the detailed plant layout and design for all of the IGCC-CLC processes with the five different OCs and three configurations (a–c). In all 15 cases, an entrained flow gasifier operating at 30 atm is fed with pulverised coal particles from the top. A 95% (vol.) pure O_2 stream at 2.35 bar is generated in a stand-alone ASU, which is then used for gasification of coal in the gasifier (Cormos, 2010b). The O_2 from the ASU is compressed to 36 atm before being fed to the gasifier (Chiesa et al., 2005), which is 1.2-times the pressure in the gasifier. The purge nitrogen (N_2) exits at 2.35 atm from the ASU. In configurations "a" and "b" (Cases 1a–5a and Cases 1b–5b), the purge N_2 stream from the ASU is not utilised anywhere in the process and could possibly be used in other industries such as the chemical, petroleum and steel (Pogrel, 1993; Evison and Gilchrist, 1992; Gavriljuk, 1996; Woolman, 1970). However, factors such as demand and purity of N_2 needs to be carefully analysed (out of the scope of this work) in order to check the effective usability of the N_2 generated in the cases studied in this work. In configuration "c" (Cases 1c–5c), this N_2 stream is further compressed to 31 atm and fed to the air reactor, to eventually expand in the expander/GT for energy recovery. The gasification of coal gives a flame temperature of 1300 °C, which is above the melting point of ash. The temperature inside the gasifier is maintained at 1300 °C by using high-pressure (HP) water for excess heat extraction, which is converted into HP steam and utilised for power generation. The melted slag flows down through the walls of the gasifier and exits from the bottom. The syngas produced after coal gasification also leaves at the bottom of the gasifier. The composition of the product stream or raw syngas stream from the gasifier is estimated from the chemical equilibrium at 1300 °C.

The raw syngas is cooled to ~30 °C in the heat recovery steam generation (HRSG) unit that solidifies and removes slag before sending it to a scrubber to remove particulate matter. The heat recovered from the syngas cooling is used for steam generation and reheating. Prior to syngas combustion and CO_2 capture, sulphur dioxide (SO_2), hydrogen sulphide (H_2S) and carbonyl sulphide (COS) are 99.5–99.9% removed from the syngas by a physical absorption method using Selexol. The HRSG unit produces the steam required for Selexol regeneration in H_2S clean up unit. The Claus plant receives the eliminated H_2S and oxidises it to elemental sulphur. Syngas after sulphur removal is passed through a heat exchanger unit where it is heated to 350 °C before being sent into the CLC fuel reactor, which is maintained at 750 °C and 30 atm. Any excess heat released in fuel reactor is extracted by pressurised water flowing through a membrane wall around the reactor. The fuel reactor is usually operated in adiabatic mode whereas, we have used an isothermal mode of operation. This is because the adiabatic mode was observed to provide widely varying temperature values (between a range of 750 and 1050 °C) in the fuel reactor for the five different OCs. Therefore, in order to maintain consistency in the flowsheet models for all five OCs, we have kept the fuel reactor at a constant temperature (750 °C) by operating it at isothermal mode using pressurised water-cooling. The syngas is fed from the bottom of the fuel reactor while OC enters from the top. The counter-current fluidised bed fuel reactor converts CO and H_2 in syngas to CO_2 and H_2O. The type of OC used in the cases discussed in this study would be copper, cobalt, iron, manganese or nickel oxides depending on the case number (shown in Table 2). It is assumed in all the cases that there is no gas leakage from the fuel reactor into the air reactor. Eqs. (1)–(5) show the reactions for syngas conversion or the main reactions occurring for each of the five OCs in the fuel reactor at 750 °C at 30 atm. A chemical and phase equilibrium model (based on Gibbs free energy minimisation) used for

Table 3
Design assumptions used for developing the CLC process flowsheet models in Aspen plus (Chiesa et al., 2005; Cleeton et al., 2009; Cormos, 2010a, 2012; Erlach et al., 2011).

Unit	Parameters
Air Separation Unit	Oxygen purity: 95% (vol.) ASU oxygen and nitrogen delivery pressure: 2.37 atm Power consumption: 225 kWh/t O_2 Oxygen and nitrogen compressor efficiency: 83%
Gasifier reactor (entrained flow shell)	Oxygen/coal ratio (kg/kg): 0.867 O_2 pressure to gasifier: 36 atm Gasification pressure: 30 atm Gasification temperature: 1300 °C (slagging conditions) Carbon conversion: 99.9% No pressure drop Gas cooling: Radiative and conductive heat exchanger Electric power for gasification aux.: 1% of input fuel LHV HP steam raised in Gasification Island: 124 bar/600 °C
Acid Gas Removal (AGR) unit for H_2S capture	Solvent: Selexol® (dimethyl ethers of polyethylene glycol) Overall H_2S removal yield: 99.5–99.9% Solvent regeneration: thermal (heat)
Chemical looping combustion unit	Fuel reactor parameters: 30 atm/750 °C Air reactor parameters: 30 atm/950 °C Gibbs free energy minimisation model for both reactors No pressure drop
CO_2 compression and drying	Delivery pressure: 150 atm Delivery temperature: 40 °C Compressor efficiency: 85% CO_2 removal yield: 100%
Expander/GT	Isentropic efficiency: 88%; Expander/GT number: 1 Discharge pressure: 1.05 atm; Pressure ratio: 28.57 Turbine inlet temperature (TIT): 950 °C Turbine outlet temperature (TOT): 500–550 °C
Steam turbines and HRSG	Three level pressures (HP/IP/LP): 124/30/6.5 bar Isentropic efficiency: 86% IP and LP reheat to 600 °C Condenser pressure: 0.046 bar Integration of steam generated in gasification island, syngas treatment, combined cycle expander/GT chemical looping unit ΔT_{min}=10 °C with no pressure drop

Table 4
Physical and chemical properties of Illinois #6 coal (Fan, 2010b; Zeng et al., 2012).

Items	Weight as received (%)	Dry weight (%)
Proximity analysis		
Moisture	11.12	–
Fixed carbon	44.19	49.72
Volatiles	34.99	39.37
Ash	9.70	10.91
Total	100.00	100.00
HHV(MJ/kg)	27.13	30.53
Ultimate analysis		
Moisture	11.12	–
Ash	9.70	10.91
Carbon	63.75	71.72
H_2	4.5	5.06
N_2	1.25	1.41
Chlorine	0.29	0.33
Sulphur	2.51	2.82
O_2	6.88	7.75
Sulphate analysis		
Pyritic	–	1.70
Sulphate	–	0.02
Organic	–	1.10

simulation of the fuel reactor obtained a CO and H_2 conversion rate of ~100% for copper-, iron-, manganese- and nickel-based OCs and 97.0–97.5% for cobalt-based OCs. Similar results for conversion efficiencies are reported by previous studies (Chiu and Ku, 2012; Cormos, 2012; Jerndal et al., 2006). For cases with copper-, cobalt-, manganese- and nickel-based OCs, the model of the fuel reactor is developed using a single RGIBBS reactor unit in Aspen plus which can perform the reactions represented by Eqs. (1)–(4). In the case of iron-based OCs, two RGIBBS reactor units are required to model the fuel reactor since a single unit cannot completely convert Fe_2O_3 into FeO, as is shown in Eq. (5) (Bohn et al., 2008; Jerndal et al., 2006). The Fe_2O_3 is first converted to Fe_3O_4 in the first RGIBBS reactor and then Fe_3O_4 is converted to FeO in the second RGIBBS reactor (Cleeton et al., 2009). Further details can be found in our previous publication (Mukherjee et al., 2014).

$$2CuO + CO + H_2 \rightarrow 2Cu + CO_2 + H_2O \quad (1)$$

$$2CoO + CO + H_2 \rightarrow 2Co + CO_2 + H_2O \quad (2)$$

$$2Mn_2O_3 + CO + H_2 \rightarrow 4MnO + CO_2 + H_2O \quad (3)$$

$$2NiO + CO + H_2 \rightarrow 2Ni + CO_2 + H_2O \quad (4)$$

$$2Fe_2O_3 + CO + H_2 \rightarrow 4FeO + CO_2 + H_2O \quad (5)$$

The OC (Me_xO_y) is progressively reduced into Me_xO_{y-1} during the syngas conversion process. In our analysis, the conversion of fuel by the OC in the CLC fuel reactor could be endothermic or exothermic depending upon the type of OC and fuel used (Hallberg et al., 2011). In our IGCC-CLC processes, the net reactions taking place in the CLC fuel reactor are exothermic at 750 °C for all the OCs studied except the iron-based OC (see Table 5). Excess heat generated is extracted by pressurised water. This heat is later

used in the Rankine cycle for power generation. In case of iron-based OCs, the net reaction in the CLC fuel reactor is endothermic, therefore it requires an external heat source. This heat is supplied by high temperature regenerated iron oxides at 950 °C coming from the air reactor. The heat required for the endothermic reactions in case of iron-based OC is less than the heat supplied by regenerated iron oxides. This indicates the availability of some excess heat in the fuel reactor of IGCC-CLC processes using iron-based OCs, which is further used in the Rankine cycle.

The high temperature and HP exhaust gas from the fuel reactor, which mainly consists of CO_2 and H_2O, is cooled to 35 °C in the HRSG unit. The water is removed by condensation leaving a pure stream of CO_2 for compression. The reduced OC particles exiting from the bottom of the fuel reactor are conveyed to the air reactor that operates within a turbulent fluidisation regime. A compressed air stream at 32 atm is used in the air reactor to re-oxidise or regenerate the OC particles. This compressed air also helps in circulation of the OC particles between the fuel reactor and the air reactor. In the air reactor, the OC is fully oxidised to Me_xO_y through Eq. (6), generating a substantial amount of heat.

$$Me_xO_{y-1} + \tfrac{1}{2}O_2 \rightarrow Me_xO_y \quad (6)$$

The operating temperature of the air reactor is maintained at 950 °C. Excess heat generated in the air reactor is removed by HP water (in configuration "a"), excess air (in configuration "b") and both excess air and N_2 supply (in configuration "c"). In configuration "a", the HP water is supplied through the membrane wall, which gradually converts to steam as it flows through air reactor and is used in the Rankine cycle for power generation. In configuration "b", an excess amount of air (i.e. more than what is actually required for complete regeneration and circulation of OC particles) is supplied to maintain the required temperature. In configuration "c", some amount of excess air used for cooling purpose in configuration "b" is replaced by N_2 from the ASU that serves the same purpose as a cooling agent. Fully oxidised OC exits from the top of the air reactor, along with hot exhaust air. The OC is separated from the air in a cyclone separator and falls in to the fuel reactor, while the high temperature and HP air is passed through a GT. The exhaust from the GT at 500–550 °C is sent to the HRSG unit for heat recovery. Section 2.2 provides a more detailed description of steam generation in the process. Details on the composition and thermodynamic state of key process streams are given in Supplementary Information (SI) Table S1 for Case 3c as an example. The CLC reactor models developed in our study are validated with experimental results available in the literature (Adanez et al., 2012; Chen et al., 2011; Chiu and Ku, 2012; Fan, 2010a; Johansson et al., 2006a; Mattisson et al., 2006). It is worth noting that all IGCC-CLC processes modelled in our study are completely thermally integrated, meaning that no external energy input is used except the coal feedstock.

2.2. Steam and water cycle details

This section describes the approach followed for steam generation and power production through the Rankine cycle in all the IGCC-CLC processes. The water and steam cycle details for Case 3a using iron-based OC are presented in Table 6, as an example case. The mass and energy balances have been established for each process unit (i.e. compressors, gasifiers, heat exchangers, turbines, H_2S removal units and the CLC reactors) to assess the performances of gas or steam cycles. The pressurised steam in the system for all three configurations (a–c) is generated through a two-step process (Chiesa et al., 2005). In configuration "a" (Cases 1a–5a), step one uses the excess heat generated in the gasifier, air reactor and fuel reactor and produces only HP steam at 600 °C and 124 bar. This helps in maintaining the required operating temperature in the vessels. In configurations "b" and "c" (Cases 1b–5b and 1c–5c), the HP steam in step one is produced by using the excess heat generated only in the gasifier and the fuel reactor since the air reactor is cooled by excess air supply (or by both air and N_2 in configuration "c") and not by HP water.

The steam generation approach followed in the second step is similar for all three configurations (a–c). In the second step, heat available from the cooling of all the exiting gaseous streams from reactors and GT (i.e. syngas stream from gasifier, exhaust from fuel reactor, and exhaust air from the GT) is used in the HRSG unit for

Table 5
Reduction (in fuel reactor) and oxidation (in air reactor) reaction enthalpies of the OCs at 750 °C and 950 °C, respectively (Barin, 1989; Barin et al., 1989).

Reduction of oxygen carrier	$\Delta H_{r,\ reduction}$ at 750 °C	Units	Oxidation of oxygen carrier	$\Delta H_{r,\ oxidation}$ at 950 °C	Units
$CuO+CO \rightarrow Cu+CO_2$	−132.29	(kJ/mol of CuO)	$0.5O_2+Cu \rightarrow CuO$	−148.44	(kJ/mol of CuO)
$CuO+H_2 \rightarrow Cu+H_2O$	−97.79				
$CoO+CO \rightarrow Co+CO_2$	−49.62	(kJ/mol of CoO)	$0.5O_2+Co \rightarrow CoO$	−233.14	(kJ/mol of CoO)
$CoO+H_2 \rightarrow Co+H_2O$	−15.13				
$Fe_2O_3+CO \rightarrow 2FeO+CO_2$	−5.37	(kJ/mol of Fe_2O_3)	$0.5O_2+2FeO \rightarrow Fe_2O_3$	−275.47	(kJ/mol of Fe_2O_3)
$Fe_2O_3+H_2 \rightarrow 2FeO+H_2O$	29.13				
$Mn_2O_3+CO \rightarrow 2MnO+CO_2$	−97.49	(kJ/mol of Mn_2O_3)	$0.5O_2+2MnO \rightarrow Mn_2O_3$	−182.29	(kJ/mol of Mn_2O_3)
$Mn_2O_3+H_2 \rightarrow 2MnO+H_2O$	−62.99				

Note: The ΔH_r values are calculated by an interpolation method.

Table 6
Water and steam cycle details for Case 3a.

Stream	Flow rate (t/h)	Inlet temperature (°C)	Outlet temperature (°C)	Pressure (bar)
HP steam produced from gasifier, fuel reactor and air reactor combined	668.52	25.0	600.0	124.0
HP steam from HRSG	82.98	25.0	600.0	124.0
HP steam to HP ST	771.5	600.0	382.2	124.0
IP steam to IP reheater	771.5	382.2	600.0	30.0
IP steam to IP ST	771.5	600.0	384.0	30.0
LP steam to LP reheater	771.5	384.0	600.0	6.5
LP steam to LP ST	771.5	600.0	32.5	6.5
Cooling water to steam condenser	43,200.0	15.0	25.5	2.0
Condensate return to HRSG	82.98	25.0	600.0	124.0

generating HP steam at 600 °C and for reheating intermediate pressure (IP) and low pressure (LP) steam to up to 600 °C. The HP steam produced in both steps is mixed before expanding it through HP ST. The exhaust of the LP ST exits at 0.046 bar and 90.5 °C (Cormos, 2012). It is then condensed to 25 °C using cooling water at an inlet temperature of 15 °C and pumped back to the process after pressure being raised to 124 bar. Supplementary Information (SI) Figs. S1 and S2 show the heat transfer diagram for Cases 3a and 3c, respectively, as an example.

2.3. Aspen Plus model

The key parameters and operating conditions used to develop the flowsheet models are summarised in Tables 2–4. Material streams used in the models involve conventional, non-conventional and solid components; therefore, MIXCINC is selected as the stream case for all cases. The Peng–Robinson–Boston–Mathias (PR–BM) property method is used for the conventional components (Aspentech, 2010). This method uses the Peng–Robinson cubic equation of state with the Boston–Mathias alpha function for all thermodynamic properties (Aspentech, 2001, 2010). General coal enthalpy (HCOALGEN) and coal density (DCOALIGT) models are used for the non-conventional components coal and ash, respectively. Each OC is entered as a solid in the component list. The RGIBBS reactor block is used for modelling coal gasifier, fuel reactor and air reactor reactors. The RGIBBS reactor restricts each reaction to equilibrium and does not consider the reaction kinetics. The main inputs given to the RGIBBS are temperature, pressure, stream flow rate and composition. The feed water in the process is pressurised by using a simple PUMP model that has an efficiency of 90%. A counter-current MHeatX type heat exchanger is used for the HRSG. A four-stage adiabatic MCOMPR type compressor in the Aspen Plus is used to compress the gas streams. Further information on the Aspen Plus modelling of the IGCC-CLC process can be found in our recent work (Mukherjee et al., 2014).

3. Results and discussions

3.1. Comparison of different OCs for power generation in IGCC-CLC process with water-cooling of CLC air reactor (Cases 1a–5a)

This section discusses and compares the performance of the five-studied OCs for the IGCC-CLC process under configuration “a” (Cases 1a–5a). Table 7 shows the parameters which are mainly of interest such as power output, power consumption and efficiency for the Cases 1a–5a. Results indicate that, cases with cobalt-based (Case 2a) and nickel-based (Case 5a) OCs achieve 97–97.5% and 99.5% syngas conversion efficiency, respectively, compared to 100% conversion efficiency for cases with copper-, iron- and manganese-based OCs. These syngas conversion efficiencies obtained by the equilibrium reactor models (RGIBBS reactor model in Aspen plus) for CLC fuel reactors in our simulations are similar to efficiencies given in Jerndal et al. (2006) and Chiu and Ku (2012). As described in Section 2.1, all the cases are based on the assumption that there is no leakage of gas from the CLC fuel reactor to air reactor. Therefore, the unconverted syngas released from CLC fuel reactors, in IGCC-CLC processes using cobalt- and nickel-based OCs, is compressed and stored along with CO_2.

Except Case 2a, all other cases under configuration “a” (Cases 1a, 3a–5a) achieve nearly the same net electrical efficiency of 32.1–32.2%. The GT in Cases 1a and 3a–5a generates 34.0 MW of power. This is because Cases 1a and 3a–5a are supplied with the same amount of pressurised hot air (30 atm; 950 °C) in their GTs, since the air required for OC regeneration in the air reactor is the same in these cases. The overall heat generated by combined oxidation and reduction reactions in the two CLC reactors is almost the same for all the OCs (see Table 5), which is not surprising as the net reaction is essentially the combustion of the syngas fuel regardless of which OC is used (Hallberg et al., 2011). Consequently, the heat available from CLC reactors for steam generation, which is a difference between total heat available from the two reactors and the heat carried away by the exhaust of air reactor to the GT, is nearly the same in all the cases under configuration “a” (except Case 2a due to incomplete fuel conversion). Besides, the heat available from the gasifier and other process streams for steam production is equal and common to all the cases. Owing to the above reasons, an approximately equal amount of steam is generated in the Rankine cycle for Cases 1a and 3a–5a giving a combined ST power output between 390.4 and 392.1 MW, which is not a significant variation considering the scale of the power plant. The power consumption by ancillaries comprising ASU, pumps and compressors ranging from 62.6 to 62.9 MW is quite similar for all cases under configuration “a”. All these factors account for the similar efficiencies achieved by Cases 1a and 3a–5a.

Unlike Cases 1a and 3a–5a, Case 2a generates less overall heat from the combined oxidation and reduction reactions in the two CLC reactors due to incomplete syngas conversion. As a result, 7–9 MW lower overall power output and 0.6–0.7% lower net electrical efficiency is exhibited compared to Cases 1a and 3a–5a. The exergetic efficiency obtained for Cases 1a–5a ranges between 28.2% and 28.9%. The CO_2 capture efficiency is ~100% for all cases independent of the OC used. Cases 1a and 4a produces 1.107 MWh of electricity per ton of CO_2 captured, which is the highest amidst all cases under configuration “a”. Cases 2a produce the lowest (1.101 MWh) amount of electricity per ton of CO_2 captured. The above discussion infers that for a specific operating temperature, the IGCC-CLC process with water-cooling of the CLC air reactor achieves the same net electrical efficiency irrespective of the type of OC used, provided all OCs have the same conversion efficiency.

Incomplete syngas conversion resulting in CO and H_2 accumulation in the compressed CO_2 stream of Cases 2a and 5a reduces (i) the purity of the sequestration ready CO_2 stream, and (ii) the total power output due to fuel wastage. The latter is further examined to determine the amount of energy which can be recovered by utilising the unconverted CO. To attain this, Cases 2a and 5a were fitted with an extra combustor unit after the CLC fuel reactor to burn the unconverted syngas and extract all the available energy from it in the form of heat. The extra heat generated by burning un-converted syngas sequentially allows producing more steam in the HRSG unit and hence more power from the STs. The extra combustor unit uses a pure O_2 stream from the ASU to aid CO and H_2 conversion to CO_2 and H_2O, respectively. This improvised design increased the overall net electrical efficiency of Case 2a (with cobalt-based OC) to 32.2% matching the efficiencies of Cases 1a and 3a–5a. No significant difference in the net electrical efficiency was observed in Case 5a with the nickel-based OC. Carbon capture efficiency remained unaffected with the addition of an extra combustor unit. In our analysis of configuration “a” (as summarised in Table 7), Cases 2a and 5a were considered without using the extra combustor (i.e. no further combustion of the unconverted syngas) in order to maintain consistency in the configuration for fair comparison. Addition of an extra combustor unit will incur extra capital cost and its usage will have economic implications.

3.2. Comparison of IGCC-CLC process (Cases 1a–5a) with the base case and other CO_2 capture technologies.

The conventional IGCC power plant considered in this study is devoid of any CO_2 capture (base case) and has a net electrical efficiency of 41.4% (see Table 7) which is significantly higher than Cases 1a–5a. No power is utilised to capture and compress CO_2 in the base case, which accounts for its higher efficiency. A

Table 7
Plant performance indicators for Cases 1a–5a obtained by Aspen plus simulations.

Plant data	Units	Base case	Copper Case 1a	Cobalt Case 2a	Iron Case 3a	Manganese Case 4a	Nickel Case 5a
Fuel Input, LHV (A)	MWth	1126.5	1126.5	1126.5	1126.5	1126.5	1126.5
CO conversion efficiency	%	–	100.0	97.5	100.0	100.0	99.5
H_2 conversion efficiency	%	–	100.0	97.0	100.0	100.0	99.4
Net expander/GT output	MWe	319.7	34.0	33.3	34.0	34.0	34.0
ST output	MWe	224.7	392.1	384.1	390.6	392.1	390.4
Gross electric power output (B)	MWe	544.4	426.1	417.4	424.6	426.1	424.4
ASU consumption + oxygen compression	MWe	34.1	34.1	34.1	34.1	34.1	34.1
CO_2 capture and compression	MWe		9.9	9.7	9.9	9.9	9.9
Power cycle pumps	MWe	3.0	4.9	4.8	4.8	4.8	4.8
Other	MWe	40.5	14.0	14.0	14.0	14.0	14.0
Total ancillary power consumption (C)	MWe	77.6	62.9	62.6	62.8	62.8	62.8
Net electric power output (D = B − C)	MWe	466.8	363.2	354.8	361.8	363.3	361.6
Gross electrical efficiency (B/A × 100)	%	48.3	37.8	37.0	37.7	37.8	37.7
Net electrical efficiency (D/A × 100)	%	41.4	32.2	31.5	32.1	32.2	32.1
Overall plant exergetic efficiency	%	37.1	28.9	28.2	28.8	28.9	28.8
CO_2 capture efficiency	%	–	~100	~100	~100	~100	~100
CO_2 captured	t/h		328.1	322.2	328.3	328.2	328.1
Power output per ton of CO_2 captured	MW/t	–	1.107	1.101	1.102	1.107	1.102

Table 8
Amount of CO_2 captured per unit net power and efficiency penalty for the IGCC-CLC processes (Cases 1a–5a) with reference to the base case.

Plant data	Units	Copper Case 1a	Cobalt Case 2a	Iron Case 3a	Manganese Case 4a	Nickel Case 5a
Net power penalty (A)	MW	103.7	112.0	105.1	103.6	105.1
CO_2 captured (B)	t/h	328.1	322.2	328.3	328.2	328.1
CO_2 captured per MW decrease in energy production than the base case (C = B/A)	t/MWh	3.16	2.87	3.12	3.16	3.12
Net electrical efficiency (D)	%	32.2	31.5	32.1	32.2	32.1
Net electrical efficiency penalty compared to base case (E = 41.4 − D)	%	9.2	9.9	9.3	9.2	9.3
Relative decrease in net electrical efficiency compared to the base case (F = E*100/41.4)	%	22.2	23.9	22.5	22.2	22.5
CO_2 captured per unit decrease in net electrical efficiency from base case (B/E)	t	35.6	32.5	35.3	35.6	35.2

comparison of the net electrical efficiency penalty of base case with Cases 1a–5a is shown in Table 8. All efficiency penalties or differences mentioned below, unless marked "relative", refer to absolute change in percentage points between the two compared cases. Cases 1a–5a has a net electrical efficiency penalty of 9.2–9.9% points compared to base case, due to a net power penalty of 103.6–112 MW associated to the CO_2 capture and compression. The drop in the net electrical efficiencies (9.2–9.9% points) for our IGCC-CLC processes in Cases 1a–5a with reference to the base case fits into the observed range for other CO_2 capture technologies (Goto et al., 2013; IEA, 2011; Kanniche et al., 2010; Leung et al., 2014). These findings are supported by Hanak et al. (2014), Xu et al. (2014) and IEA (2011) by reporting a drop of ~10%, 11–16% and 10–12% points in the net electrical efficiency, respectively, for a supercritical coal-fired power plant using monoethanolamine (MEA) based post-combustion CO_2 capture technology. A drop of 14.5–15.0% points in the net electrical efficiency was observed by Sanpasertparnich et al. (2010) and Kanniche et al. (2010) for pulverised coal power plants using amine based post-combustion CO_2 capture technology. Kanniche et al. (2010), Urech et al. (2014) and IEA (2011) have reported a drop of 9%, 8.6% and 8.3% points in the net electrical efficiency, respectively, for IGCC processes using physical solvent based pre-combustion capture technologies, which is lower than that for the IGCC-CLC processes in Cases 1a–5a. However, the IGCC-CLC processes studied can achieve a greater (~100%) CO_2 capture rate compared to 85–95% for pre- and post-combustion capture technologies (Chiesa et al., 2005; Cormos, 2012; IEA, 2011). In summary, the IGCC-CLC processes (Cases 1a–5a) operating at a moderate temperature range of 750–950 °C with water-cooling of the CLC air reactor can outperform post-combustion CO_2 capture technology. However, these IGCC-CLC processes can be further optimised.

3.3. *Comparison of different OCs for power generation in IGCC-CLC process with air-cooling of CLC air reactor (Cases 1b–5b).*

Results for IGCC-CLC processes with air-cooling of the CLC air reactor (Configuration "b" or Cases 1b–5b) having different OCs are shown in Table 9. Cases 1b–5b mentioned further are identical to cases 1a–5a except the adaptation of water-cooling at the CLC air reactor as the means to maintain the temperature at 950 °C inside the reactor (see Section 2).

Case 3b generates the highest power output of 191.5 MW in the GT (combined cycle) followed by Cases 2b, 5b, 4b and 1b with 164.9, 163.7, 124.4 and 91.7 MW, respectively (see Table 9). Case 3b uses an iron-based OC that has a reaction enthalpy of 275.47 kJ/mol for oxidation with air, which is highest amongst all five OCs. This indicates Case 3b generates more heat in the air reactor that is used to feed the GT and therefore the GT in Case 3b produces more power compared to other cases. The GT power output trend for Cases 1b–5b corresponds to oxidation reaction enthalpies ($\Delta H_{r,\ oxidation}$) of OC with air (see Table 5). For the Rankine cycle, Case 1b produced the highest power of 340.7 MW from the STs followed by Cases 4b, 5b, 2b and 3b with 311.6, 275.1, 267.0 and 250.4 MW, respectively. The interpretation for such high power generation in the STs can be the copper-based OC used in Case 1b having the highest reduction reaction enthalpy ($\Delta H_{r,\ reduction}$) of 230.1 kJ/mol when reduced with syngas (indicating highest heat production in the fuel reactor), compared to Cases 2b, 3b, 4b and 5b. Similar to the GT power output trend, the STs power output follows values of

Table 9
Plant performance indicators for Cases 1b–5b obtained by Aspen plus simulations.

Plant Data	Units	Copper Case 1b	Cobalt Case 2b	Iron Case 3b	Manganese Case 4b	Nickel Case 5b
Fuel input, LHV (A)	MWth	1126.5	1126.5	1126.5	1126.5	1126.5
CO conversion efficiency	%	100.0	97.5	100.0	100.0	99.5
H_2 conversion efficiency	%	100.0	97.0	100.0	100.0	99.4
Net expander/GT output	MWe	91.7	164.9	191.5	124.4	163.7
ST output	MWe	340.7	267.0	250.4	311.6	275.1
Gross electric power output (B)	MWe	432.2	431.9	441.9	436.0	438.8
ASU consumption + oxygen compression	MWe	34.1	34.1	34.1	34.1	34.1
CO_2 capture and compression	MWe	9.9	9.7	9.9	9.9	9.9
Power cycle pumps	MWe	4.4	3.7	3.6	4.1	3.8
Other	MWe	14.0	14.0	14.0	14.0	14.0
Total ancillary power consumption (C)	MWe	62.4	61.5	61.6	62.1	61.8
Net electric power output (D = B − C)	MWe	369.8	370.4	380.3	373.9	377.0
Gross electrical efficiency (B/A × 100)	%	38.4	38.3	39.2	38.7	38.9
Net electrical efficiency (D/A × 100)	%	32.8	32.9	33.7	33.2	33.4
Overall plant exergetic efficiency	%	29.4	29.5	30.3	29.8	30.0
CO_2 capture efficiency	%	~100	~100	~100	~100	~100
CO_2 captured	t/h	328.1	322.2	328.3	328.2	328.1
Power output per ton of CO_2 captured	MW/t	1.127	1.150	1.159	1.139	1.150

reduction reaction enthalpies ($\Delta H_{r,\ reduction}$), except Case 2b that uses a cobalt-based OC, due to incomplete fuel conversion (see Table 5). Case 3b achieves the highest net electrical efficiency of 33.7% compared to all other cases under configuration "b" even after generating the lowest power from the STs. In contrast to that, Case 1b has the lowest 32.8% net electrical efficiency even though it generates the highest power from the STs.

The above discussion allows to conclude that generating more heat in the air reactor is preferable to generate it in the fuel reactor in order to obtain higher net electrical efficiency in IGCC-CLC processes with air-cooling of the CLC air reactor. This is because the heat generated in the air reactor is utilised in an efficient manner in a combined cycle. The heat generated in the fuel reactor is used in a comparatively less efficient Rankine cycle. This demonstrates that OCs with higher $\Delta H_{r,\ oxidation}$ values (e.g. iron oxides) are preferred for IGCC-CLC process with air-cooling. It follows that the OCs with higher values of $\Delta H_{r,\ oxidation}$ (e.g. copper oxides) are the less preferred since these indicate a lower value for $\Delta H_{r,\ oxidation}$ (Note: $\Delta H_r = \Delta H_{r,\ oxidation} + \Delta H_{r,\ reduction}$, which is approximately constant for all OCs; see Table 5). It was found from the analysis of Cases 1b–5b that a direct comparison of oxidation and reduction reaction enthalpy values for different OCs can cogently predict their performances for the IGCC-CLC process with air-cooling of the CLC air reactor.

3.4. Effect of air-cooling against water-cooling on the power output of IGCC-CLC processes

The effect of air-cooling against water-cooling of the CLC air reactor for power output in the IGCC-CLC process is analysed by comparing net electrical efficiencies of Cases 1b–5b with Cases 1a–5a (see Table 10). No significant difference in net electrical efficiency was observed in all water-cooling cases, except Case 2a with Cobalt-based OC (see Section 3.1). This exception can be attributed to incomplete syngas conversion. In contrast, the air-cooling cases (Cases 1b–5b) show a difference of 0.9% points in net electrical efficiency. Results suggest that the use of air-cooling (as opposed to water-cooling) increases the net electrical efficiency of the IGCC-CLC process by 0.6–1.6% points for all of the OCs. However, a fixed air supply to air reactor prevents the water-cooling cases from effectively utilising the heat generated via the efficient combined cycle (GT) at 950 °C. Instead, a considerable amount of heat is used in the less efficient Rankine cycle (STs) operating at 600 °C. In contrast, the air-cooling cases allow the utilisation of all the heat generated in the air reactor in the combined cycle and then the remaining heat from the fuel reactor in the Rankine cycle. Case 3b achieves a highest relative increase (5%) in net electrical efficiency (see Table 10), whereas Case 1b shows the lowest (1.9%) increase. Compared to Cases 2b–5b, Case 1b generates less heat in the air reactor due to lower enthalpy of reaction (148.44 kJ/mol) for oxidation of copper with air (see Table 5). It indicates that only a small amount of heat is available to recover in the air reactor of Case 1b. This explains why Case 1b obtains the minimum advantage of air-cooling in comparison with Cases 2b–5b. On the other hand, iron, with the highest enthalpy of oxidation reaction allows Case 3b to completely exploit air-cooling the available excess heat, which was earlier used in the Rankine cycle in Case 3a, in an efficient combined cycle.

Fig. 3 shows a power output comparison of water- and air-cooling cases by using Case 3a and 3b (both the cases use iron-based OC) as example cases. It can be seen from Fig. 3 that generating more power in the GT (i.e. giving preference to the combined cycle or GT for power generation as in Case 3b) ultimately leads to higher net power production. The IGCC-CLC processes with air-cooling (Cases 1b–5b) can capture relatively 2.3–4.7% more CO_2 per MW of net power output in comparison to IGCC-CLC processes with water-cooling (Cases 1a–5a). To conclude, the use of air-cooling of the air reactor instead of water-cooling can improve the net power output or net electrical efficiency of the process. However, it is accompanied by an economic disadvantage caused by an increased size of air reactor, air-compressor, gas–solid separator and GT resulting in higher capital cost of the plant. A techno-economic comparison, which is beyond the scope of present work, can provide further details on the suitability of the oxygen carriers.

3.5. Effect of ASU integration to CLC air reactor on the power output of IGCC-CLC process

In ASU integration to the CLC air reactor, the N_2 from the ASU is compressed to 32 atm and used in the air reactor to maintain the required temperature of 950 °C inside the reactor. The N_2, along with other exhaust gases from the air reactor, is vented through the GT to the atmosphere. The former Cases 1a–5a and 1b–5b were modified to Cases 1c–5c to analyse the effect of ASU integration of the CLC air reactor on the net power output of the IGCC-CLC process. Here, the effects of N_2 as a cooling agent in addition to air-cooling of the reactor were investigated. Table 11

presents the performance indicators for Cases 1c–5c while the results in Table 12 show the change in the net electrical efficiency of the IGCC-CLC processes after ASU integration.

The ASU integration to the air reactor increased the net electrical efficiency of the IGCC-CLC process by 0.5–0.6% points despite the additional work required for N_2 compression (see Table 12). The IGCC-CLC processes in Cases 1b–5b has air-cooling, which uses compressed atmospheric air at 32 atm. However, for the IGCC-CLC processes with air-cooling and ASU integration (Cases 1c–5c), atmospheric air is partially replaced by N_2 from the ASU, which is already compressed to 2.67 atm. Hence, the IGCC-CLC process in Cases 1c–5c saves a part of the compression work, ultimately resulting in higher net electrical efficiency than the IGCC-CLC processes in Cases 1b–5b. The overall comparison of results from Tables 7, 9 and 11 indicate that configuration "c" with air-cooling along with ASU integration is the most efficient among all three configurations (a–c). Furthermore, Case 3c with the iron-based OC has the highest efficiency of 34.3% compared to all other IGCC-CLC cases (15 cases) evaluated in this work. The net electrical efficiencies obtained in our IGCC-CLC processes (Cases 1c–5c) are ~1.2–10% points lower than those observed in other studies given in Table 1. This is mainly because the studies summarised in Table 1 use only iron- or nickel-based OCs and are consequently studied at comparatively higher temperatures (1050–1300 °C) for the CLC air reactor and hence at higher turbine inlet temperature (TIT). However, in order to allow comparison with copper-based OCs (with a low melting point of 1085 °C) in our analysis, we have fixed the maximum temperature to 950 °C in our models.

Table 10
Effect of air-cooling against water-cooling on the net electrical efficiency of the IGCC-CLC process.

Oxygen carrier	Net electrical efficiency (%)			
	Fully water cooled (A, Cases 1a–5a from Table 7)	Fully air cooled (B, Cases 1b–5b from Table 9)	Difference in efficiencies, (**C=B−A**)	Relative increase in efficiency (%), ($\frac{C}{A}\times 100$)
Copper	32.2	32.8	0.6	1.9
Cobalt	31.5	32.9	1.4	4.4
Iron	32.1	33.7	1.6	5.0
Manganese	32.2	33.2	1.0	3.1
Nickel	32.1	33.4	1.3	4.0

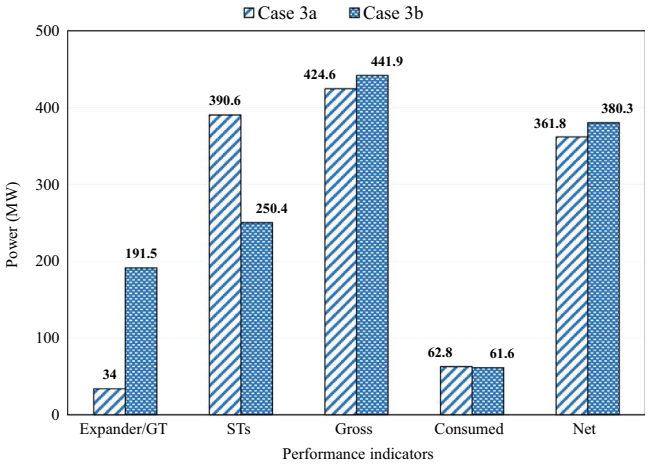

Fig. 3. Relation between GT, ST, gross, consumed and net power output for Case 3a (water-cooling) and Case 3b (air-cooling).

3.6. Comparison of IGCC-CLC process with air-cooling and ASU integration of CLC air-reactor (Cases 1c–5c) with the base case

Results obtained from IGCC-CLC processes with air-cooling and ASU integration of the CLC air reactor in Cases 1c–5c are compared with the base case to analyse energy and efficiency penalties associated with the CO_2 capture (see Table 13). Case 3c showed a net power penalty of 80.1 MW and net electrical efficiency penalty of 7.1% points, which is the lowest among all other cases in configuration "c". On the other hand, Case 1c shows the maximum energy and net electrical efficiency penalty of 90.7 MW and 8.1%, respectively. Case 3c captures 4.1 t per hour of CO_2 per MW decrease in energy production compared with base case whilst Cases 1c, 2c, 4c and 5c captures 3.6, 3.5, 3.7 and 3.9 t of CO_2, respectively. Comparative studies of Cases 1c–5c demonstrate that iron-based OCs can capture 4.8–14.6% relatively more CO_2 per MW of net power penalty than the copper-, cobalt-, manganese- and nickel-based OCs.

Fig. 4 shows that the IGCC-CLC processes can generate 24.0–118.9 MW more power than the base case in the Rankine cycle (STs). However, in the combined cycle (GT), the IGCC-CLC processes generates 89.0–193.8 MW less power than the base case. The base case operates at comparatively higher temperature

Table 11
Plant performance indicators for Cases 1c–5c obtained by Aspen plus simulations.

Plant Data	Units	Copper Case 1c	Cobalt Case 2c	Iron Case 3c	Manganese Case 4c	Nickel Case 5c
Fuel input, LHV (A)	MW	1126.5	1126.5	1126.5	1126.5	1126.5
CO conversion efficiency	%	100.0	97.5	100.0	100.0	99.5
H_2 conversion efficiency	%	100.0	97.0	100.0	100.0	99.4
Net expander/GT output	MWe	125.9	204.2	230.7	163.6	203.0
ST output	MWe	343.6	265.3	248.7	309.8	273.0
Gross electric power output (B)	MWe	469.5	469.5	479.4	473.5	476.0
ASU consumption+oxygen compression	MWe	34.1	34.1	34.1	34.1	34.1
CO_2 capture and compression	MWe	9.9	9.7	10.2	9.9	9.8
Power cycle pumps	MWe	4.4	3.7	3.5	4.1	3.7
Other	MWe	45.0	45.0	45.0	45.0	45.0
Total ancillary power consumption (C)	MWe	93.4	92.5	92.8	93.1	92.7
Net electric power output (D=B−C)	MWe	376.1	377.0	386.7	380.3	383.2
Gross electrical efficiency ($B/A\times 100$)	%	41.6	41.6	42.5	42.0	42.2
Net electrical efficiency ($D/A\times 100$)	%	33.3	33.4	34.3	33.7	34.0
Overall plant exergetic efficiency	%	29.9	30.0	30.7	30.2	30.5
CO_2 capture efficiency	%	~100	~99.9	~100	~100	~99.9
CO_2 captured	t/h	328.1	322.2	328.3	328.2	328.1
Power output per ton of CO_2 captured	MW/t	1.14	1.17	1.17	1.15	1.16

(1300 °C) in the combined cycle leading to higher power output in the GT. However, the IGCC-CLC processes in our study operate at 950 °C, which is constrained by the melting point of the copper oxide OC carrier studied. OCs made from metals such as iron and nickel can allow operating CLC at temperatures above 950 °C and thus, are more promising than the copper-based OCs as far as chemical- and phase-equilibrium for reactions is concerned.

Fig. 5 shows that the modification from water-cooling to air-cooling along with the ASU integration further improve the performance of IGCC-CLC processes since it increases the net electrical efficiency from 31.5% to 32.2% (in Cases 1a–5a) to 33.3–34.3% (in Cases 1c–5c). Hence, this modification reduces the net electrical efficiency penalty from 9.2% to 9.9% (in Cases 1a–5a) to 7.1–8.1% points (see Table 13) and makes the IGCC-CLC process more efficient than pre-combustion capture technology, which has a net electrical efficiency penalty between 8.3% and 9.0% points (see Section 3.2).

4. Summary and conclusion

This work compares five different OCs (copper, cobalt, iron, manganese and nickel oxides) for the IGCC-CLC process. The overall power output, net power penalty for CO_2 capture and net electrical efficiency are the key parameters used for comparison. The effects of water-cooling, air-cooling and ASU integration of the CLC air reactor on the performance of the IGCC-CLC process are critically examined. To achieve the above objectives, 15 different flowsheet models of the IGCC-CLC process were developed in a chemical process simulation tool "Aspen Plus". In addition, a conventional IGCC process without CO_2 capture was developed to estimate the penalties associated with CO_2 capture in the IGCC-CLC processes. Comparisons of the performance of the modelled systems were made against pre- and post-combustion CO_2 capture technologies based on the data available in literature. The results obtained show that:

- Air-cooling of the CLC air reactor is preferred to water-cooling because air-cooling can more effectively utilise the heat generated in the CLC reactor system in a combined cycle (GT) with a superior efficiency. In contrast, the water-cooling cases uses a significant amount of heat generated in the CLC reactors in a less efficient Rankine cycle (STs), which ultimately results in 1.6% points lower net electrical efficiency compared with air-cooling cases.
- The IGCC-CLC processes with air-cooling and ASU integration achieve a net electrical efficiency of 33.3–34.3%. This efficiency is 0.6% points and 2.1% points higher than the IGCC-CLC processes with only air-cooling and only water-cooling, respectively.
- The direct comparison of oxidation and reduction reaction enthalpies of the OCs can be useful to predict the performance of different OCs for an IGCC-CLC process. The OCs with higher values of reaction enthalpy for oxidation with air ($\Delta H_{r,\ oxidation}$) and high melting points are preferred for the IGCC-CLC process.
- The high $\Delta H_{r,\ oxidation}$ value allows an iron-based OC to achieve a net electrical efficiency of 34.3% for the IGCC-CLC process, which is the highest amongst all five OCs. This makes the iron-based OC more favourable for the IGCC-CLC process than the other four OCs, as far as chemical and phase equilibriums are concerned.
- The IGCC-CLC process shows a net electrical efficiency penalty of 7.1–8.1% points with reference to a conventional IGCC process w/o CO_2 capture. A comparison of these efficiency penalty values with the literature indicates that the IGCC-CLC

Table 12
Relation between cases with and without the ASU integration for CLC process.

Oxygen carrier	Net electrical efficiency without ASU integration, (Y; %) **Cases 1b–5b** (*values taken from* Table 9)	Net electrical efficiency with ASU integration, (X;%) **Cases 1c–5c** (*values taken from* Table 11)	Difference in efficiencies ($Z=X-Y$; %)	Relative increase in efficiency (%), ($\frac{Z}{Y}\times 100$)
Copper	32.8	33.3	0.5	1.5
Cobalt	32.9	33.4	0.5	1.5
Iron	33.7	34.3	0.6	1.8
Manganese	33.2	33.7	0.5	1.5
Nickel	33.4	34.0	0.6	1.8

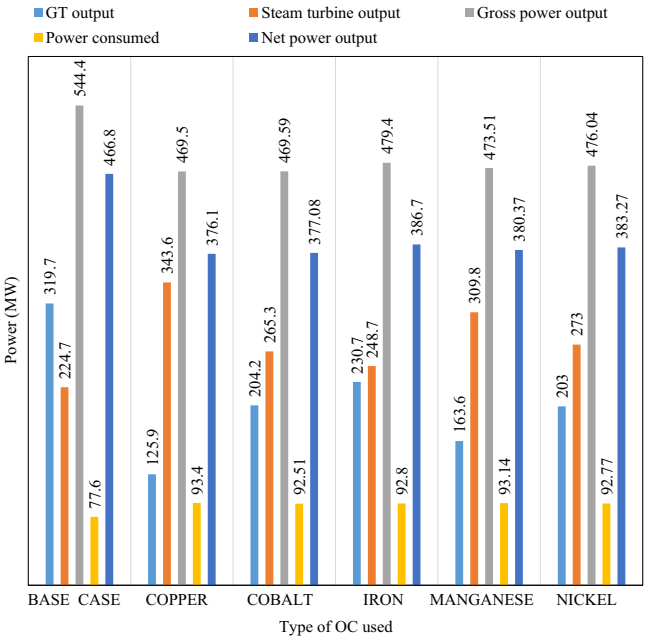

Fig. 4. Relation between gross power output, power consumed and net power output for Cases 1c–5c, against the base case.

Table 13
Amount of CO_2 captured per unit net power and efficiency penalty for the IGCC-CLC cases (cases 1c–5c) with reference to the base case.

Plant Data	Units	Copper Case 1c	Cobalt Case 2c	Iron Case 3c	Manganese Case 4c	Nickel Case 5c
Net power penalty (A)	MW	90.7	89.8	80.1	86.5	83.6
CO_2 captured (B)	t/h	328.1	322.2	328.3	328.2	328.1
CO_2 captured per MW decrease in energy production than the base case (C=B/A)	t/MWh	3.6	3.5	4.1	3.7	3.9
Net electrical efficiency (D)	%	33.3	33.4	34.3	33.7	34.0
Net electrical efficiency penalty compared to base case (E=41.4−D)	%	8.1	8.0	7.1	7.7	7.4
Relative decrease in net electrical efficiency compared to the base case (F=E*100/41.4)	%	19.5	19.3	17.1	18.5	17.8
CO_2 captured per unit decrease in net electrical efficiency from base case (B/E)	t	40.5	40.2	46.2	42.5	44.3

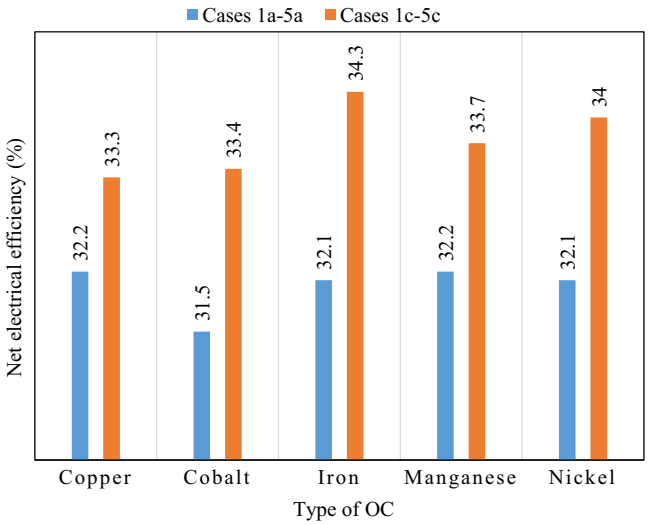

Fig. 5. Comparison between the net electrical efficiencies of Cases 1a–5a and Cases 1c–5c.

process, using copper-, cobalt-, iron-, manganese- and nickel-based OCs, is more efficient than the amine based post-combustion capture technology and equally efficient as the solvent based pre-combustion capture technology.

The findings from this work demonstrate a relationship between reaction enthalpies (reaction with air; $\Delta H_{r,\ oxidation}$ and syngas; $\Delta H_{r,\ reduction}$) of different OCs and power output for the IGCC-CLC process. Further analysis on the comparison of OCs could be performed by considering the detailed reaction kinetics and deactivation rates of different OCs, which can highly influence the cost of the overall process. This is however out of the scope of our current work and is a topic to be considered by future studies. The chemical and phase equilibrium approach assumed in this work for the OC and fuel conversion reactions can help in developing a critical understanding of the IGCC-CLC process with regard to different OCs.

Conflict of interest

The authors declare no competing financial interest.

Acknowledgement

This work is carried out within the joint UK–China EPSRC project (Grant reference: EP/I010912/1) titled as "Multi-scale evaluation of advanced technologies for capturing the CO_2: Chemical looping applied to solid fuels". The authors thank Dr. Stuart Scott from the University of Cambridge for providing useful suggestions on the manuscript. P.K. thanks the consortium members from the Universities of Cambridge, Nottingham, Tsinghua and South-East for their cooperation. The Surrey team is also grateful to the Department of Civil and Environmental Engineering at the University of Surrey for additional funding support for this work.

Appendix A. Supporting information

Supplementary data associated with this article can be found in the online version at http://dx.doi.org/10.1016/j.ces.2015.03.009.

References

Adánez, J., de Diego, L.F., García-Labiano, F., Gayán, P., Abad, A., Palacios, J.M., 2004. Selection of oxygen carriers for chemical-looping combustion. Energy Fuels 18, 371–377.
Adanez, J., Abad, A., Garcia-Labiano, F., Gayan, P., de Diego, L.F., 2012. Progress in chemical-looping combustion and reforming technologies. Prog. Energy Combust. Sci. 38, 215–282.
Anheden, M., 2000. Analysis of Gas Turbine Systems for Sustainable Energy Conversion (Ph.D. Thesis). Royal Institute of Technology, Sweden p. 71.
Anheden, M., Svedberg, G., 1996. Chemical-looping combustion in combination with integrated coal gasification—a way to avoid CO_2 emission from coal fired power plants without a significant decrease in net power efficiency. In: Proceedings of the Energy Conversion Engineering Conference, 1996. IECEC '96, Proceedings of the 31st Intersociety, vol. 2043. pp. 2045–2050.
Anheden, M., Svedberg, G., 1998. Exergy analysis of chemical-looping combustion systems. Energy Convers. Manag. 39, 1967–1980.
Arjmand, M., 2014. Copper and Manganese-based Oxygen Carriers in Chemical-looping combustion (CLC) and Chemical-looping with Oxygen Uncoupling (CLOU) (Ph.D. Thesis). Chalmers University of Technology, Göteborg p. 81.
Arjmand, M., Leion, H., Mattisson, T., Lyngfelt, A., 2014. Investigation of different manganese ores as oxygen carriers in chemical-looping combustion (CLC) for solid fuels. Appl. Energy 113, 1883–1894.
Aspentech, 2001. Physical Property Methods and Models. Aspen Physical Property System 11.1, Cambridge, USA p. 436.
Aspentech, 2010. Physical Property Methods. Aspen Physical Property System, Burlington, USA p. 240.
Bao, J., Li, Z., Cai, N., 2014. Interaction between iron-based oxygen carrier and four coal ashes during chemical looping combustion. Appl. Energy 115, 549–558.
Barin, I., 1989. Thermochemical Data of Pure Substances – Part I. Wiley-VCH, New York, USA p. 916.
Barin, I., Sauert, F., Ernst'Schultze-Rhonhof, Sheng, W.S., 1989. Thermochemical Data of Pure Substances – Part II. Wiley-VCH, New York, USA p. 993.
Bhavsar, S., Tackett, B., Veser, G., 2014. Evaluation of iron- and manganese-based mono- and mixed-metallic oxygen carriers for chemical looping combustion. Fuel 136, 268–279.
Bohn, C.D., Müller, C.R., Cleeton, J.P., Hayhurst, A.N., Davidson, J.F., Scott, S.A., Dennis, J.S., 2008. Production of very pure hydrogen with simultaneous capture of carbon dioxide using the redox reactions of iron oxides in packed beds. Ind. Eng. Chem. Res. 47, 7623–7630.
Boot-Handford, M.E., Abanades, J.C., Anthony, E.J., Blunt, M.J., Brandani, S., Mac Dowell, N., Fernandez, J.R., Ferrari, M.-C., Gross, R., Hallett, J.P., Haszeldine, R.S., Heptonstall, P., Lyngfelt, A., Makuch, Z., Mangano, E., Porter, R.T.J., Pourkashanian, M., Rochelle, G.T., Shah, N., Yao, J.G., Fennell, P.S., 2014. Carbon capture and storage update. Energy Environ. Sci. 7, 130–189.
Cabello, A., Abad, A., García-Labiano, F., Gayán, P., de Diego, L.F., Adánez, J., 2014. Kinetic determination of a highly reactive impregnated Fe_2O_3/Al_2O_3 oxygen carrier for use in gas-fueled chemical looping combustion. Chem. Eng. J. 258, 265–280.
Chen, S., Xiang, W., Xue, Z., Sun, X., 2011. Experimental investigation of chemical looping hydrogen generation using iron oxides in a batch fluidized bed. Proc. Combust. Inst. 33, 2691–2699.
Chiesa, P., Consonni, S., Kreutz, T., Robert, W., 2005. Co-production of hydrogen, electricity and CO_2 from coal with commercially ready technology. Part A: Performance and emissions. Int. J. Hydrog. Energy 30, 747–767.
Chiu, P.-C., Ku, Y., 2012. Chemical looping process – a novel technology for inherent CO_2 capture. Aerosol Air Qual. Res. 12, 1421–1432.
Cho, P., 2005. Development and Characterisation of Oxygen-Carrier Materials for Chemical-Looping Combustion (Ph.D. Thesis). Chalmers University of Technology, Göteborg, Sweden p. 67.
Cho, P., Mattisson, T., Lyngfelt, A., 2004. Comparison of iron-, nickel-, copper- and manganese-based oxygen carriers for chemical-looping combustion. Fuel 83, 1215–1225.
Cleeton, J.P.E., Bohn, C.D., Müller, C.R., Dennis, J.S., Scott, S.A., 2009. Clean hydrogen production and electricity from coal via chemical looping: identifying a suitable operating regime. Int. J. Hydrog. Energy 34, 1–12.
Cormos, C.-C., 2010a. Evaluation of energy integration aspects for IGCC-based hydrogen and electricity co-production with carbon capture and storage. Int. J. Hydrog. Energy 35, 7485–7497.
Cormos, C.-C., 2010b. Evaluation of iron based chemical looping for hydrogen and electricity co-production by gasification process with carbon capture and storage. Int. J. Hydrog. Energy 35, 2278–2289.
Cormos, C.-C., 2012. Evaluation of syngas-based chemical looping applications for hydrogen and power co-generation with CCS. Int. J. Hydrog. Energy 37, 13371–13386.
de Diego, L.F., García-Labiano, F., Adánez, J., Gayán, P., Abad, A., Corbella, B.M., María Palacios, J., 2004. Development of Cu-based oxygen carriers for chemical-looping combustion. Fuel 83, 1749–1757.
de Diego, L.F., García-Labiano, F., Gayán, P., Abad, A., Cabello, A., Adánez, J., Sprachmann, G., 2014. Performance of Cu- and Fe-based oxygen carriers in a 500 Wth CLC unit for sour gas combustion with high H_2S content. Int. J. Greenh. Gas Control. 28, 168–179.
Erlach, B., Schmidt, M., Tsatsaronis, G., 2011. Comparison of carbon capture IGCC with pre-combustion decarbonisation and with chemical-looping combustion. Energy 36, 3804–3815.

Evison, B., Gilchrist, R., 1992. New developments in nitrogen in the oil industry. In: Proceedings of the Society of Petroleum Engineers (SPE) Mid-Continent Gas Symposium, 13–14 April, 1992, Amarillo, TX.
Fan, L., 2010a. Chemical Looping Systems for Fossil Energy Conversions. Wiley-AIChe, USA p. 420.
Fan, L., Zeng, L., Wang, W., Luo, S., 2012. Chemical looping processes for CO_2 capture and carbonaceous fuel conversion – prospect and opportunity. Energy Environ. Sci. 5, 7254–7280.
Fang, H., Haibin, L., Zengli, Z., 2009. Advancements in development of chemical-looping combustion: a review. Int. J. Chem. Eng., 16, Article ID 710515, http://dx.doi.org/10.1155/2009/710515.
Fossdal, A., Bakken, E., Øye, B.A., Schøning, C., Kaus, I., Mokkelbost, T., Larring, Y., 2011. Study of inexpensive oxygen carriers for chemical looping combustion. Int. J. Greenh. Gas Control. 5, 483–488.
Gao, Z., Shen, L., Xiao, J., Qing, C., Song, Q., 2008. Use of coal as fuel for chemical-looping combustion with Ni-based oxygen carrier. Ind. Eng. Chem. Res. 47, 9279–9287.
Gavriljuk, V., 1996. High nitrogen steels. Nitrogen in iron and steel. ISIJ Int. 36, 738–745.
Goto, K., Yogo, K., Higashii, T., 2013. A review of efficiency penalty in a coal-fired power plant with post-combustion CO_2 capture. Appl. Energy 111, 710–720.
Hallberg, P., Leion, H., Lyngfelt, A., 2011. A method for determination of reaction enthalpy of oxygen carriers for chemical looping combustion – application to ilmenite. Thermochim. Acta 524, 62–67.
Hamers, H., Romano, M., Spallina, V., Chiesa, P., Gallucci, F., Annaland, M., 2014. Comparison on process efficiency for CLC of syngas operated in packed bed and fluidized bed reactors. Int. J. Greenh. Gas Control. 28, 65–78.
Hanak, D.P., Biliyok, C., Yeung, H., Białecki, R., 2014. Heat integration and exergy analysis for a supercritical high-ash coal-fired power plant integrated with a post-combustion carbon capture process. Fuel 134, 126–139.
Hossain, M.M., de Lasa, H.I., 2007. Reactivity and stability of Co–Ni/Al_2O_3 oxygen carrier in multicycle CLC. AIChE J. 53, 1817–1829.
Hossain, M.M., de Lasa, H.I., 2008. Chemical-looping combustion (CLC) for inherent separations—a review. Chem. Eng. Sci. 63, 4433–4451.
IEA, 2011. Cost and Performance of Carbon Dioxide Capture from Power Generation, France. 51 pp. Available from: ⟨http://www.iea.org/publications/freepublications/publication/costperf_ccs_powergen.pdf⟩ (accessed 04.06.14).
IEA, 2013. CO_2 emissions from fuel combustion. IEA. 158 pp. Available from: ⟨http://www.iea.org/publications/freepublications/publication/co2emissionsfromfuelcombustionhighlights2013.pdf⟩ (accessed 04.06.14).
IPCC, 2013. IPCC Fifth Assessment Report: Climate Change 2013 (AR5). 1552 pp. Available from: ⟨http://www.climatechange2013.org/images/report/WG1AR5_ALL_FINAL.pdf⟩ (accessed 14.06.14).
IPCC, 2014. Climate Change 2014: mitigation of climate change. In: Edenhofer, O., Pichs-Madruga, R., Sokona, Y., Farahani, E., Kadner, S., Seyboth, K., Adler, A., Baum, I., Brunner, S., Eickemeier, P., Kriemann, B., Savolainen, J., Schlömer, S., von Stechow, C., Zwickel, T., Minx, J.C. (Eds.), Contribution of Working Group III to the Fifth Assessment Report of the Intergovernmental Panel on Climate Change. Cambridge University Press, Cambridge, UK; New York, NY, USA.
Imtiaz, Q., Hosseini, D., Müller, C.R., 2013. Review of oxygen carriers for chemical looping with oxygen uncoupling (CLOU): thermodynamics, material development, and synthesis. Energy Technol. 1, 633–647.
Jerndal, E., Mattisson, T., Lyngfelt, A., 2006. Thermal analysis of chemical-looping combustion. Chem. Eng. Res. Des. 84, 795–806.
Jing, D., Mattisson, T., Ryden, M., Hallberg, P., Hedayati, A., Van Noyen, J., Snijkers, F., Lyngfelt, A., 2013. Innovative oxygen carrier materials for chemical-looping combustion. Energy Procedia 37, 645–653.
Johansson, E., Mattisson, T., Lyngfelt, A., Thunman, H., 2006a. Combustion of syngas and natural gas in a 300 W chemical-looping combustor. Chem. Eng. Res. Des. 84, 819–827.
Johansson, M., Mattisson, T., Andersb, L., 2006b. Comparison of oxygen carriers for chemical-looping combustion. Therm. Sci. 10 (3), 93–107.
Kanniche, M., Gros-Bonnivard, R., Jaud, P., Valle-Marcos, J., Amann, J.-M., Bouallou, C., 2010. Pre-combustion, post-combustion and oxy-combustion in thermal power plant for CO_2 capture. Appl. Therm. Eng. 30, 53–62.
Kumar, P., Saroj, D.P., 2014. Water–energy–pollution nexus for growing cities. Urban Clim. 10, 846–853.
Leung, D.Y.C., Caramanna, G., Maroto-Valer, M.M., 2014. An overview of current status of carbon dioxide capture and storage technologies. Renew. Sustain. Energy Rev. 39, 426–443.
Li, F., Fan, L.-S., 2008. Clean coal conversion processes – progress and challenges. Energy Environ. Sci. 1, 248–267.
Li, F., Zeng, L., Velazquez-Vargas, L.G., Yoscovits, Z., Fan, L.-S., 2010. Syngas chemical looping gasification process: bench-scale studies and reactor simulations. AIChE J. 56, 2186–2199.
Lyngfelt, A., Leckner, B., Mattisson, T., 2001. A fluidized-bed combustion process with inherent CO_2 separation; application of chemical-looping combustion. Chem. Eng. Sci. 56, 3101–3113.
Lyngfelt, A., Johansson, M., Mattisson, T., 2008. Chemical-looping combustion – status of development. In: Proceedings of 9th International Conference on Circulating Fluidized Bed, Hamburg, Germany.
Mattisson, T., Johansson, M., Lyngfelt, A., 2006. The use of NiO as an oxygen carrier in chemical-looping combustion. Fuel 85, 736–747.
Mukherjee, S., Kumar, P., Hosseini, A., Yang, A., Fennell, P., 2014. Comparative assessment of gasification based coal power plants with various CO2 capture technologies producing electricity and hydrogen. Energy Fuels 28, 1028–1040.
Pires, J.C.M., Martins, F.G., Alvim-Ferraz, M.C.M., Simões, M., 2011. Recent developments on carbon capture and storage: an overview. Chem. Eng. Res. Des. 89, 1446–1460.
Pogrel, M.A., 1993. The use of liquid nitrogen cryotherapy in the management of locally aggressive bone lesions. J. Oral Maxillofac. Surg. 51, 269–273.
Rezvani, S., Huang, Y., McIlveen-Wright, D., Hewitt, N., Mondol, J.D., 2009. Comparative assessment of coal fired IGCC systems with CO_2 capture using physical absorption, membrane reactors and chemical looping. Fuel 88, 2463–2472.
Sanpasertparnich, T., Idem, R., Bolea, I., deMontigny, D., Tontiwachwuthikul, P., 2010. Integration of post-combustion capture and storage into a pulverized coal-fired power plant. Int. J. Greenh. Gas Control. 4, 499–510.
Shah, K., Moghtaderi, B., Wall, T., 2012. Selection of suitable oxygen carriers for chemical looping air separation: a thermodynamic approach. Energy Fuels 26, 2038–2045.
Shulman, A., Cleverstam, E., Mattisson, T., Lyngfelt, A., 2009. Manganese/iron, manganese/nickel, and manganese/silicon oxides used in chemical-looping with oxygen uncoupling (CLOU) for combustion of methane. Energy Fuels 23, 5269–5275.
Song, H., Shah, K., Doroodchi, E., Wall, T., Moghtaderi, B., 2014. Reactivity of Al_2O_3- or SiO_2-supported Cu-, Mn-, and Co-based oxygen carriers for chemical looping air separation. Energy Fuels 28, 1284–1294.
Sorgenfrei, M., Tsatsaronis, G., 2014. Design and evaluation of an IGCC power plant using iron-based syngas chemical-looping (SCL) combustion. Appl. Energy 113, 1958–1964.
Spallina, V., Romano, M.C., Chiesa, P., Lozza, G., 2013. Integration of coal gasification and packed bed CLC process for high efficiency and near-zero emission power generation. Energy Procedia 37, 662–670.
Spallina, V., Romano, M.C., Chiesa, P., Gallucci, F., van Sint Annaland, M., Lozza, G., 2014. Integration of coal gasification and packed bed CLC for high efficiency and near-zero emission power generation. Int. J. Greenh. Gas Control. 27, 28–41.
Urech, J., Tock, L., Harkin, T., Hoadley, A., Maréchal, F., 2014. An assessment of different solvent-based capture technologies within an IGCC-CCS power plant. Energy 64, 268–276.
Wolf, J., Anheden, M., Yan, J., 2005. Comparison of nickel- and iron-based oxygen carriers in chemical looping combustion for CO_2 capture in power generation. Fuel 84, 993–1006.
Woolman, W., 1970. Processes of cleaning and passivating reactor equipment. Google Patents No. US3522093 A.
Xu, G., Hu, Y., Tang, B., Yang, Y., Zhang, K., Liu, W., 2014. Integration of the steam cycle and CO_2 capture process in a decarbonization power plant. Appl. Therm. Eng. 73, 275–284.
Zeng, L., He, F., Li, F., Fan, L.-S., 2012. Coal-direct chemical looping gasification for hydrogen production: reactor modeling and process simulation. Energy Fuels 26, 3680–3690.